J Mater Sci (2014) 49:7669–7678
DOI 10.1007/s10853-014-8475-x

Infiltration of tin bronze into alumina particle beds: influence of alloy chemistry on drainage curves

Alain Léger · Ludger Weber · Andreas Mortensen

Received: 2 May 2014 / Accepted: 14 July 2014 / Published online: 31 July 2014

Abstract The wetting of angular alumina particle preforms by Cu–Sn alloys is investigated by means of pressure infiltration experiments conducted at 1150 °C, using a system enabling dynamic and precise measurements of the metal volume injected into the preform. Wetting is quantified in terms of drainage curves, which plot the volume fraction of molten metal in the packed powder preform (also called saturation) versus the applied pressure. The shape of the curves confirms earlier findings, namely (i) the initial stage of infiltration is dominated by percolation and obeys a universal scaling relation while the metal shape is fractal; and (ii) at higher saturation, incremental pore-filling is dictated by local pore geometrical characteristics, saturation curves obeying then the Brooks–Corey correlation. According to sessile drop data in the literature, the Cu–Sn system is characterized by relatively small changes in the contact angle with alloy composition (128°–122°), while the metal surface tension changes by more than a factor two over the whole composition range. One would, therefore, expect that the drainage curves be indifferently proportional to the molten metal surface tension or the work of immersion: the present data show that this is indeed verified.

Introduction

Capillary forces have importance in many diverse materials processes, such as casting, solidification, bonding, or composite material fabrication [1–3]. An important example is infiltration, which is one of the main processes used to produce composite materials: in infiltration, open pores of a reinforcement body (usually called a *preform*) are filled with a fluid material that will make the matrix of the composite once it has solidified [4–17]. Infiltration is one of the main ways in which metal matrix composites (MMCs) are produced [4–11, 15, 18–20]. Because the wetting of solid reinforcements by molten metals is usually poor, spontaneous infiltration is rarely possible with MMCs. Also, given the high interfacial area created during this process and the high value of the liquid surface tension of metals [11], capillary forces are directly apparent: these are manifest as a pressure-resisting ingress of the metal into the preform, and are one of the main issues in the fabrication of MMCs.

Capillarity in materials processing is most often quantified in terms of the equilibrium wetting angle θ of the relevant liquid over a flat solid surface in a surrounding (generally gaseous) atmosphere. The values of θ, together with that of the liquid surface tension σ_{LV}, are derived, respectively, from a (generally isotropic) capillary equilibrium written along the solid plane and expressed as the Young equation, and from a derivation of the drop shape within the gravitational field [1–3, 21]. These two basic capillary parameters are, however, insufficient to fully characterize wetting in infiltration processing: the complex 3D labyrinth defined by irregularly shaped open pores of the preforms makes the problem geometrically far more complex than that of a drop along a flat surface, or of a meniscus flowing in a straight capillary tube. Also, wetting being dynamic in infiltration, if there is any kinetic interaction between the solid and the liquid, relevant values of θ or σ_{LV} might differ from those measured in the more static sessile drop experiment. As a result, in infiltration and in porous media fluid flow more generally, wetting is measured not using a few scalar quantities (such as θ, σ_{LV}, and an average pore size) but by means of continuous curves, which trace the evolution of the capillary pressure as the

A. Léger (✉) · L. Weber · A. Mortensen
Laboratory of Mechanical Metallurgy, EPFL, Station 12, 1015 Lausanne, Switzerland
e-mail: alain.leger@epfl.ch

molten metal gradually invades the porous preform to be infiltrated. These curves are known as *drainage/imbibition curves*, and plot the volume fraction of pore space filled by the invading fluid (saturation, S) versus the pressure difference P between the fluid and the initial atmosphere in the pores [5, 8, 11, 22–30]. Drainage curves are measured when a non-wetting fluid invades the porous medium; imbibition curves on the other hand result when a wetting fluid gradually fills pores of the preform.

The measurement of drainage curves relevant to metal matrix composite processing is made practically difficult by generally high temperatures and applied pressures: 1000 °C and 10 MPa are typical orders of magnitude. Various methods have nonetheless been developed to enable this [5, 8, 11, 18, 22–26, 31–34]. We use here an apparatus that tracks, dynamically and with high precision, the volume of metal that has entered a porous solid preform (as is practiced at room temperature in a mercury porosimeter) as a function of pressure and time, thus providing entire drainage curves characteristic of a given system in one, single, infiltration experiment [26, 31–33]. The apparatus comprises, in its current configuration, a custom-designed optics-based system capable of measuring the displacement of a graphite plunger that floats atop the surface of a liquid metal bath, which is pushed by pressurized gas to invade open pores of a preform situated below the metal surface [26].

In a recent article, we have brought to light the role of percolation in initial phases of slow, gradual, pressure infiltration of several different alumina or carbon preforms with pure molten copper [33]. This contribution is an extension of that work to tin bronze: we present here drainage curves that quantify the wetting during infiltration of porous Al_2O_3 preforms by Cu–Sn molten alloys, covering the entire alloy spectrum from pure Cu to pure Sn. This ceramic–metal system is interesting because of its potential for engineering application (bronze having attractive mechanical properties, particularly in bearings), but also because reliable sessile drop data exist in the literature for Cu–Sn alloys on alumina, across the entire spectrum of compositions from pure Cu to pure Sn [2, 35, 36]. This system is furthermore somewhat peculiar in that the molten metal surface tension varies significantly (by a factor 2.5) as the composition transitions from Cu to Sn, while the contact angle varies little (from 122° to 128°; corresponding to a roughly 15 % variation in $\cos\theta$). We show here that drainage curve functional characteristics found with this system are consistent with earlier work (thus confirming our finding that percolation effects dominate the initial phase of infiltration), and that measured drainage curves are shifted homothetically as the tin content varies, as should be, given the wetting characteristics of this system.

Experimental

Materials

Porous preforms were prepared from angular alumina α-Al_2O_3 F1000 particles (similar to those used in Refs. [25, 26, 33, 37]) purchased from Treibacher Schleifmittel (Laufenburg, Germany) and having an average diameter around 5 μm. Powders were packed into preforms by cold isostatic pressing (CIP) at 150 MPa during 1 min. Most CIPed preforms were cylindrical, about 14 mm in diameter and 10 mm in height. The volume fraction of ceramic in the preforms (and hence in the composites), V_r, was measured by densitometry using a Sartorius MC 210P microbalance of sensitivity ± 10 μg assuming full infiltration of the composites and found to be 0.54 ± 0.03. The specific surface of the F1000 particles was measured by nitrogen adsorption/desorption (i.e., by the BET technique) and found to be $A_s = 1160 \pm 56$ m^2/kg for the batch of powder used here.

Electrolytic tough pitch copper and 99.9 % pure tin were used as infiltrants, either as pure metals, or after blending to produce copper–tin alloys, having compositions Cu–50at.%Sn, Cu–40at.%Sn, Cu–20at.%Sn, Cu–10at.%Sn, and Cu–5at.%Sn. Alloying was conducted using a high-vacuum induction furnace under static argon.

The ceramic particle morphology was evaluated by means of scanning electron microscopy (Zeiss Merlin). The as-received powder was characterized in this way, as were particles extracted from fully infiltrated composites having a matrix of Cu–40at.%Sn, by chemical dissolution of the composite matrix in a solution of 30 ml of H_2O, 30 ml of nitric acid 65 %, and 30 ml of hydrochloric acid 32 % during 30 min. The as-received powder was also similarly immersed in the same chemical solution and characterized, so as to ensure that the particle surface was not modified during the dissolution process as a result of contact with the dissolving solution.

Infiltration experiments

Continuous infiltration

A detailed description of infiltration apparatus characteristics and of the experimental procedure can be found in Refs. [26, 33, 37]. In a few words, a CIPed preform is placed underneath a slug of metal inside a cylindrical alumina crucible in a pressure infiltration apparatus. Upon melting of the metal by induction heating while pumping a primary vacuum (around 1.5 Pa) within the apparatus, the preform becomes sealed from the surrounding atmosphere. Once the infiltration temperature has stabilized, at 1150 °C for all experiments of this work, stepwise increasing pressurized argon gas drives the molten metal into the open

pores of the preform, infiltrating it from all sides. The volume of metal entering the preform is tracked dynamically by a custom-built optics-based system that measures the movement of a graphite plunger that floats atop of the liquid metal. In the stepwise pressurization cycles used here, the pressure is increased by holding each pressure level for a time long enough that the displacement of the graphite plunger reaches a plateau, or in other words, for the saturation to stabilize. This ensures that the metal saturation and pressure are governed by capillary forces [26] with minimal influence of pressure gradients due to viscous friction; the pressure and the saturation reached after each such hold thus give one point along the saturation curve for the system at hand. Full infiltration (meaning $S = 1$) is taken to occur when, within uncertainty, the graphite plunger no longer moves after the pressure is increased, indicating that all available pores within the preform have been invaded. This procedure permits to trace the entire drainage curve after one single infiltration experiment [26, 33]. Two custom-built devices were also incorporated to provide rotative and vibrative motion of the plunger. Rotation is used before infiltration to break up any oxide skin covering the molten metal surface, while continuous horizontal vibrative motion is used to disengage the plunger during an experiment. After complete infiltration, the composite is cooled within the apparatus by switching off the heater while maintaining the applied gas pressure. For each metal, *i.e.*, either pure copper, pure tin, or one of the five different Cu-x-at.%Sn alloys ($x = 50$, 40, 20, 10, 5), two different CIPed angular F1000 preforms were infiltrated under stepwise increasing pressure.

Mercury intrusion porosimetry

A drainage curve for a preform of the same CIPed F1000 alumina particles (preform diameter = 9 mm, preform height $h = 10$ mm) was measured using a commercial mercury porosimeter (Pascal 140 and Pascal 440 de Thermo Electron Corporation now Thermo Fisher Scientific, Waltham, MA, USA) at room temperature. The maximal pressure applied was 15 MPa.

Partial infiltration

A partial infiltration experiment was also performed using a similar preform with Cu–20at.%Sn at a single, constant, pressure of 2.03 MPa, held at 1150 °C for approximately 1 h. The composite was then cooled within the apparatus while maintaining the applied gas pressure. In order to preserve the partly porous regions during metallographic preparation, the metal shell surrounding the preform was first carefully removed; then, the remaining open pores of the preforms were filled with epoxy through a drilled hole, under vacuum. The resulting sample was cut, polished, and examined in a scanning electron microscope (FEI XLF30), under backscattered electron mode (to bring out the metal). The metal/pore relative distribution and the metal fractal dimension were then measured using thresholded images from the observed two-dimensional metallographic cuts, as in Refs. [26, 33], by means of the box-counting method (using the function "Fractal box counter" of ImageJ, U. S. National Institutes of Health, Bethesda, Maryland, USA). In this method, the fractal dimension D is computed from the relation $N(h) \sim h^{-D}$, where $N(h)$ is the number of boxes of linear size h necessary to cover a data set of points distributed in a two-dimensional plane. The fractal dimension was measured around the infiltration front, where the fraction metal is lowest; nearer the preform periphery, the metal volume fraction is slightly higher, causing D to increase somewhat while the metal distribution gradually passes from a percolation-dominated geometry to a more compact shape that is governed to a higher degree by local pore geometrical characteristics [28, 29, 33, 38].

Results

Drainages curves

Figure 1 compares the drainages curves characteristic of the infiltration of CIPed Al_2O_3 preforms by pure copper, pure tin, and five different Cu-x-at.%Sn alloys ($x = 50$, 40,

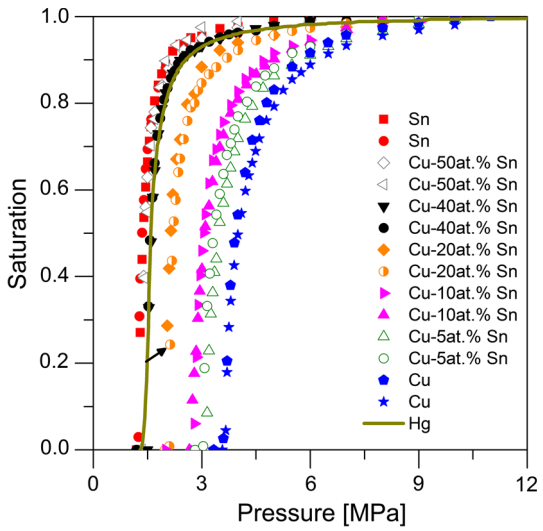

Fig. 1 Drainage curves for CIPed angular F1000 Al_2O_3 preforms made by CIP infiltrated with Sn, Cu–50at.%Sn, Cu–40at.%Sn, Cu-20at.%Sn, Cu–10at.%Sn, Cu–5at.%Sn and Cu at 1150 °C under stepwise increasing pressure and with Hg at room temperature. The *arrow* represents the final pressure applied to produce a partly infiltrated composite (Al_2O_3/Cu–20at.%Sn, 2.03 MPa during approximately 1 h)

20, 10, 5) under stepwise increasing pressure at 1150 °C, with the curve obtained using a commercial mercury intrusion porosimetry at room temperature. The black arrow in Fig. 1 represents the final pressure used to partly infiltrate a similar preform with Cu–20at.%Sn at 2.03 MPa (total saturation across the sample $S \approx 0.2$).

Characterization of the microstructure and the ceramic particles

Figure 2 shows SEM images (in backscattered electron mode) of (a) partly and (b) fully infiltrated composites with a matrix of Cu–20at.%Sn under low magnification (left) and high magnification (right). The white square represents the area used to measure the fractal dimension D_{2D} of the metal using the box-counting method following the same procedure as in Ref. [33]: the resulting value is $D_{2D} = 1.62$.

Figure 3 compares SEM images (in secondary electron mode) of the as-received initial Al_2O_3 particles (a) before and (b) after immersion in the chemical solution with (c) particles obtained after dissolution of the metallic matrix (Cu-40at.%Sn) in a fully infiltrated composite. No apparent surface modification was observed between the as-received powder before and after immersion in the chemical solution (Fig. 3a, b).

Discussion

Drainage curves

Clear and reproducible drainage curves are obtained with the present infiltration apparatus for all ceramic–metal system investigated here, as shown in Fig. 1. Infiltration of the preform starts at a metal-dependent threshold pressure P_c, progresses rapidly as P increases, then gradually approaches full saturation ($S = 1$) at significantly higher pressures.

Adding up to 50at.% tin to copper facilitates penetration of the molten metal within the open pores of the preform (as visible by a decrease of P_c with alloying). Above 50at.% Sn, the obtained drainage curves are very close to those measured with pure tin. As can be seen, the drainage curve obtained with Hg (by mercury intrusion porosimetry) at room temperature resembles those obtained for the Cu–Sn system at elevated temperature—it in fact fits almost perfectly the curve for Cu–40at.% Sn.

The microstructure of the fully infiltrated composite in Fig. 2b is typical for this class of composites after successful processing: it features a pore-free matrix surrounding contacting particles, and interfaces are free of visible reaction products.

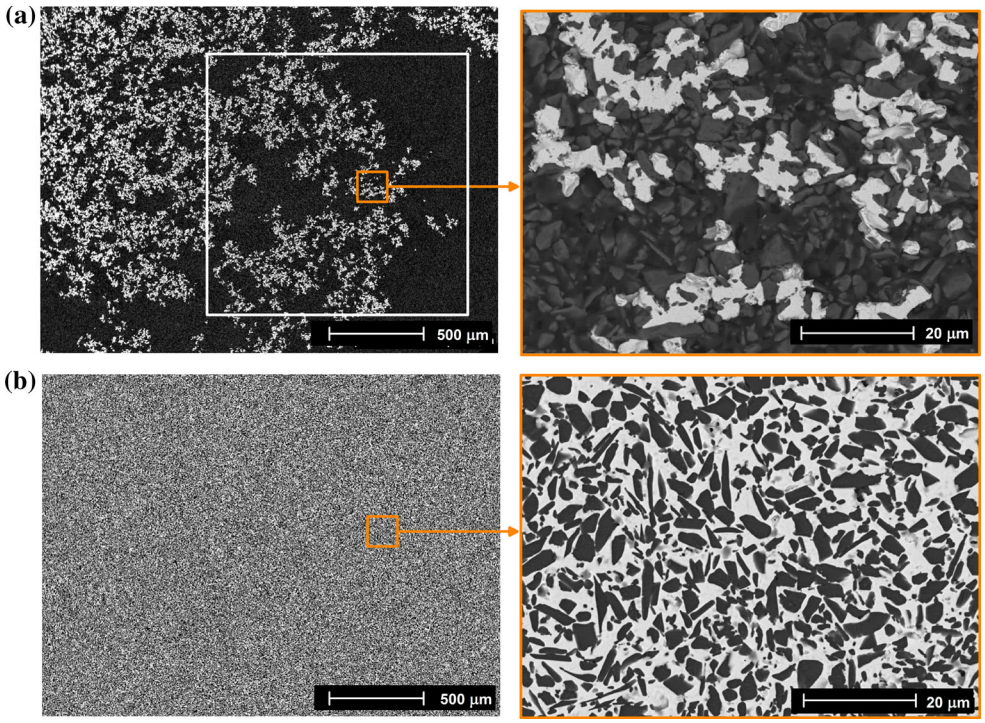

Fig. 2 Different magnification SEM images of angular F1000 alumina preforms partly **a** and fully **b** infiltrated with Cu–20at.%Sn. The final infiltration pressures are **a** 2.03 MPa and **b** 11 MPa. The white square (768 × 768 pixels) in **a** indicates the area used to measure the fractal dimension using the box-counting method (from "ImageJ" function named "Fractal box counter", size of the boxes: 2, 3, 4, 6, 8, 12, 16, 24, 32, 48, 64, 96, 128, and 192 pixels). See Ref. [33] for more details on the fractal measurement procedure

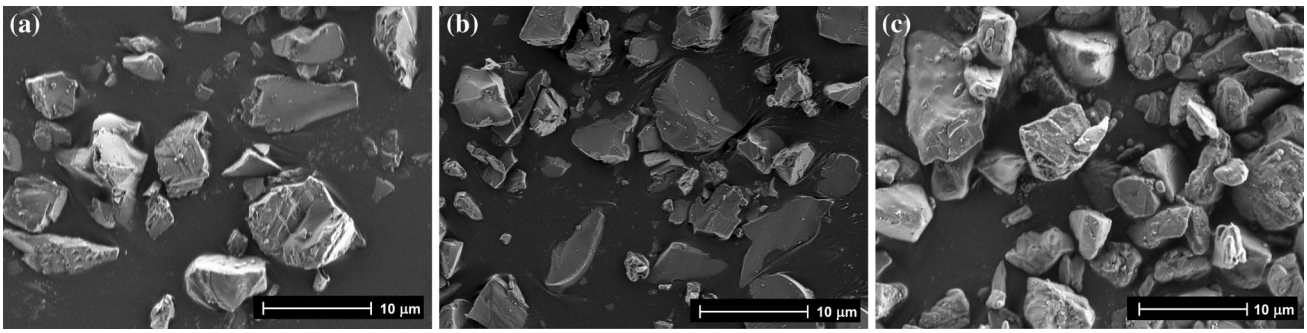

Fig. 3 SEM images in secondary electron mode of the as-received alumina F1000 particles **a** before and **b** after immersion in the chemical solution, **c** similar particles after infiltration and dissolution of the solidified Cu–40at.%Sn matrix

Initial stage of infiltration: percolation

Figure 2a shows typical examples of how complex is the flow path of the metal (white phase) within the open pores of the preforms: the metallic phase in this frozen partly infiltrated composite (F1000/Cu–20at.%Sn) is in the form of fingers of highly irregular shape, several or many pores wide, which surround other regions of uninfiltrated pores, the size of which is distributed over an equally wide range. The fingers spread in all directions, i.e., have little relation with the overall direction of fluid flow, being governed by pore size distribution and pore connectivity statistics rather than by local pore characteristics and size. These are signs that infiltration is, in this intermediate phase of the process, governed by percolation. To confirm this, drainage curves and fractal features, namely the fractal dimension of the infiltration front, are compared with prediction of percolation theory, as in Refs. [33, 39].

At the percolation threshold, computer simulation of trapping-free invasion percolation coupled with elementary reasoning leads to expect that, in the vicinity of the percolation threshold (i.e., for P just above P_c), the saturation curve will follow a universal scaling law given in Refs. [33, 39]:

$$S = C(P - P_c)^{\beta}, \tag{1}$$

where C is a system-dependent constant and $\beta = 0.41$ whatever the pore structure. When plotting the drainage curves of Fig. 1 in coordinates of $S^{(1/0.41)}$ versus P to test Eq. 1, straight lines are obtained, Fig. 4a, confirming findings of Ref. [33], namely that the initial portion of the drainage curve in metal matrix composite pressure infiltration obeys universal scaling. As in Ref. [33], here too the power law is obeyed over a large range of saturation, up to $S \approx 0.7$.

That initial phases of infiltration are governed by percolation is also confirmed by standard fractal dimensions measurement methods on 2D metallographic cuts at the infiltration front of the frozen "capillary fingering" metal formed after partial infiltration (when P is just past P_c). Percolation theory predicts an infinite cluster of fractal dimension 2.52 (in three dimensions). Using the box-counting method (for more details on the fractal measurement procedure see Ref. [33]), the fractal dimension D_{2D} was measured to be 1.62, in accordance with the value obtained for the same preform infiltrated with pure copper (D_{2D} between 1.6 and 1.7) in Ref. [33]. Since $D_{3D} = D_{2D} + 1$, this means that the cluster of invaded pores is a fractal of dimension near 2.5, as predicted by percolation theory [40–42]. The present results thus extend to Cu–Sn alloys and (as concerns only the scaling law) mercury the findings documented in Ref. [33] on the existence of an initial percolation-dominated stage in the pressure infiltration process.

Later stage of infiltration: the Brooks and Corey correlation

At higher saturation, universality is lost and the drainage curves follow a semi-empirical law known as the Brooks–Corey (BC) correlation [23, 27, 43], which has amply been documented to govern drainage curves of metal matrix composite systems [24–26, 32, 44–47]. This links the saturation S and the capillary pressure P, according to

$$S = 1 - \left(\frac{P_b}{P}\right)^{\lambda}, \tag{2}$$

where P_b is a "bubbling pressure" (related to the size of the largest pore forming a continuous network) and λ is a "pore size distribution index," which is related to the distribution of sizes of flow channels within the porous medium at hand.

The BC correlation is well obeyed in the latter portion of the present drainage curves: parallel straight lines are obtained when plotting drainage curves from Fig. 1 in $\ln(1-S)$ versus $\ln P$, Fig. 4b. The pore size distribution index λ (measured here by fitting a straight line through the data in the range $-1 > \ln(1-S) > -2$, corresponding to

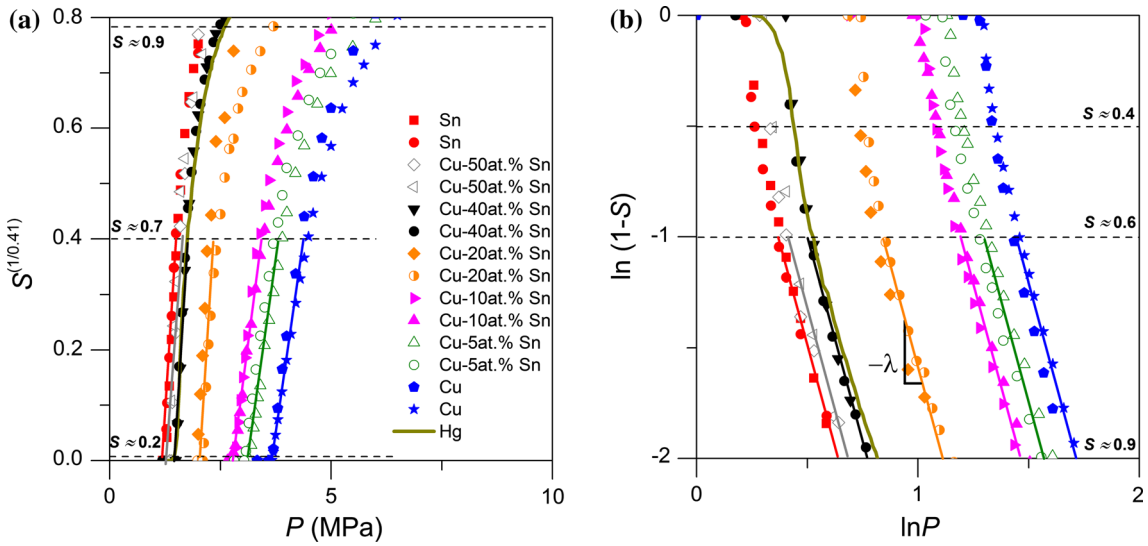

Fig. 4 Measured drainage curves for each system, plotted to test **a** the universal scaling law derived from percolation theory, Eq. 1, and **b** the semi-empirical relation proposed by Brooks and Corey, Eq. 2. The pore size distribution index λ of the latter law was measured in the range of $-1 > \ln(1-S) > -2$; this yields $\lambda = 3.7 \pm 0.4$ independently of the metal used

$0.6 \leq S \leq 0.9$) is found to be independent of the metal used: the slope is the same, at $\lambda = 3.7$, for all metals and alloys of this work, including Hg. This indicates that λ mainly reflects the characteristics of the preform (as was initially proposed by Brooks and Corey). To ensure that tin additions to copper do not alter significantly the alumina particle morphology during infiltration, as was observed with similar Al_2O_3 particles infiltrated by Cu–Al alloys at 1200 °C [48], the as-received Al_2O_3 particles were compared with particles extracted from the composite after complete dissolution of a Cu–40at.%Sn matrix using a solution that does not affect the particle morphology (Fig. 3). One finds only a slight change of the particle angularity, in that the sharpest angles and ridges are somewhat rounded after infiltration; seemingly, this slight surface modification was insufficient to modify λ in a measurable way.

Link with the surface tension and/or the work of immersion

The work of immersion W_i of a solid in a fluid,

$$W_i \equiv \sigma_{LS} - \sigma_{SV} = -\sigma_{LV} cos\theta \quad (3)$$

where σ_{LS}, σ_{SV}, and σ_{LV} are the interfacial energies between solid (S) and liquid (L), solid and vapor (V), and liquid and vapor, respectively, is the change in free energy that accompanies replacement of a unit area of solid surface with as much solid/liquid interface. Since after infiltration the liquid surface area change is generally far smaller than the interfacial area created, W_i is the thermodynamic driving force or energy barrier (depending on its sign) characteristic of the overall (reversible) infiltration process [8, 11, 49–51]. A corollary is that, if infiltration takes place without irreversible dissipation of energy, then the integral of the drainage curve equals W_i times the metal/reinforcement interfacial area per unit volume of metal.

There are, however, generally irreversible energy losses accompanying infiltration of a complex network of pores such as that found between packed monomodal-comminuted alumina particles of this work. These losses come in particular from the many local cusps in curvature experienced by the molten metal as it travels through the preform, which it invades pore by pore, in irregular "Haines jumps" each time it passes through the narrowest constrictions joining two pores, driven by a pressure that, therefore, can significantly exceed that required to invade a network of straight pores having the same total surface area [22, 23, 30]. Taken together, data from earlier work conducted on strongly non-wetting systems (θ well above 90°) show that the total measured work required to overcome capillary forces and obtain full (slow) infiltration is roughly equal to W_i times the metal/reinforcement interfacial area per unit volume of metal [25, 26, 31, 37, 47, 52–54]. This suggests in turn that (i) with such high wetting angles, irreversible energy losses during infiltration are small in comparison with the total reversible work thermodynamically required by the infiltration process in such non-wetting systems; and (ii) drainage curves are then roughly proportional to the work of immersion W_i. Here, we explore a system in which only σ_{LV} varies significantly, while θ remains relatively constant, at a value situated somewhat above 120° (Fig. 5).

Figure 5 gives literature values for σ_{LV} in Cu–Sn alloys (Fig. 5a) [35, 36] and θ for the Al_2O_3/Cu–Sn system

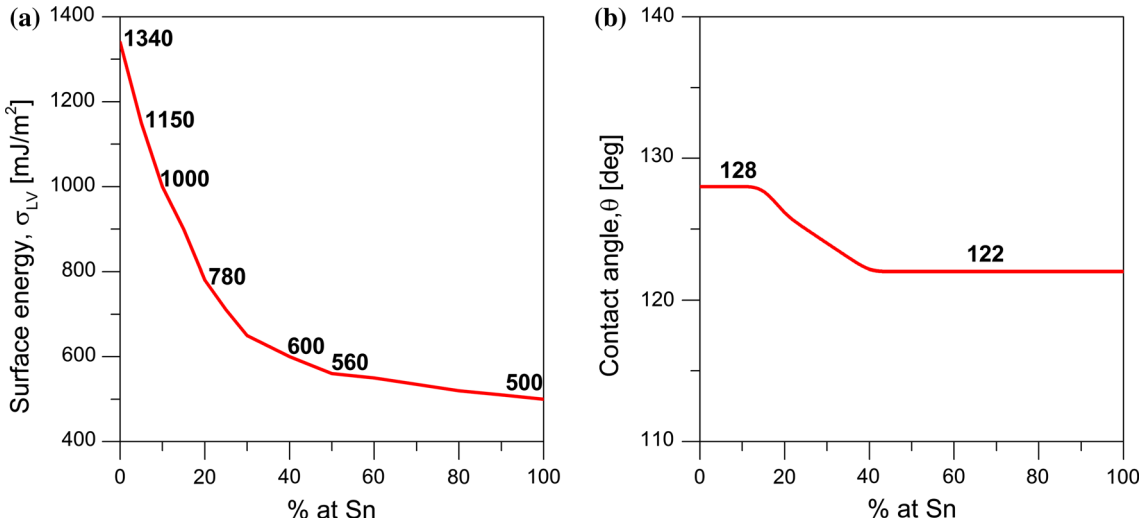

Fig. 5 **a** Liquid vapor surface energy σ_{LV} of Cu–Sn alloy at 1100–1150 °C from Refs. [35, 36] and **b** contact angle θ of alumina on Cu–Sn system at 1150 °C from [2]. Values used to normalize the drainages curves, see Fig. 6

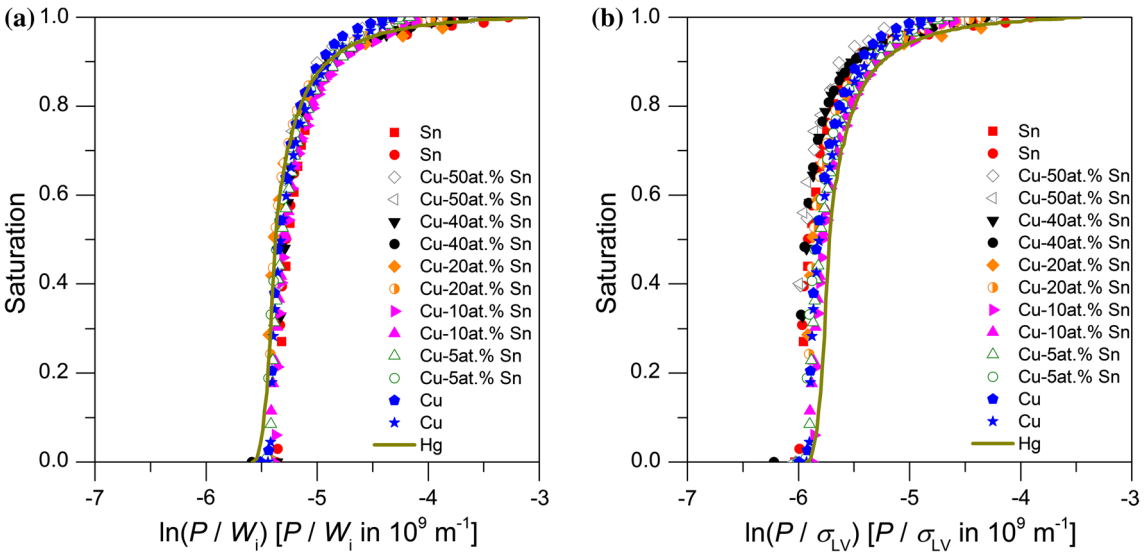

Fig. 6 **a** Drainages curves (note the logarithmic horizontal axis coordinate) normalized by a) the work of immersion W_i ($W_i = -\sigma_{LV}cos\theta$) and **b** the surface energy σ_{LV} alone. Value taken from σ_{LV} and θ come from the sessile drop experiment and are given in Fig. 5 for the Cu–Sn system. For Hg, we have taken $\sigma_{LV} = 486$ mJ/m^2 and $\theta = 135°$ (this being the median value of literature values [55, 56], which are in the range of $\theta = 127°$ to 142°)

(Fig. 5b) [2]. For mercury at room temperature, reported values for the contact angle θ on alumina range from 127° to 142° [55, 56]; an average value ($\theta = 135°$) is thus taken here. The surface tension of liquid mercury at room temperature is $\sigma_{LV} = 486$ mJ/m^2 [57]. Given the limited range of variation of cosθ across systems of the present investigation (cosθ varies from –0.52 to –0.71 as θ goes from 122 to 135°), it is relatively indifferent whether drainage curves are rescaled using W_i or σ_{LV}: as seen, after division of the pressure with either of these two scaling factors, all the drainage curves regroup relatively nicely into one single curve, Fig. 6, regardless of whether one scales these using W_i or σ_{LV}. The curve for mercury fits slightly better if one rescales by W_i instead of σ_{LV}; however, the improvement is too small to be significant, particularly in view of uncertainty on literature data for the value of θ characteristic of mercury on alumina (see above). The present data thus confirm what one would a priori expect, namely that all else constant including the wetting angle, the drainage curve scales roughly with the metal surface tension.

Finally, if we calculate for each experiment the total work required to infiltrate a unit volume of preform,

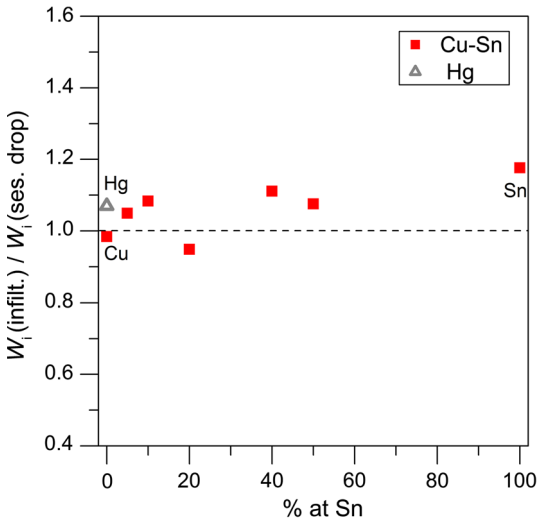

Fig. 7 Ratio of W_i according to infiltration (Eq. 5) over W_i according to sessile drop data (Eq. 3) as a function of %at Sn for Cu–Sn/Al_2O_3 at 1150 °C and Hg/Al_2O_3 at room temperature

$$W = (1 - V_r) \int_0^1 PdS, \tag{4}$$

and divide this by the total preform/infiltrant interface area created per unit volume of preform,

$$W_{i,infilt} = \frac{W}{A_S \cdot V_r \cdot \rho_{alumina}}, \tag{5}$$

where $\rho_{alumina}$ is the density of this alumina ($3.876 \cdot 10^3$ kg m^{-3} [31]), then we obtain an "apparent" work of immersion $W_{i,infilt}$ which can be compared with the value, W_i, which is deduced from sessile drop data in the literature (Eq. 3 and Fig. 5). The ratio of the two quantities is given versus composition in Fig. 7: as seen, it is near unity for all systems explored here, reaching a maximum value of 1.18 for pure tin. This implies that, for this non-wetting series of metals and alloys, replacing the solid particle surface with as much liquid/metal interface represents the majority of the energy required to effect infiltration against the (opposing) action of capillarity. Irreversible energy losses are, thus, here relatively small.

Conclusions

From the results presented in this work, the following conclusions can be drawn:

Entire drainage curves characterizing capillarity in high-temperature infiltration of porous Al_2O_3 preforms by Cu–Sn alloys across the entire composition range at 1150 °C can be obtained with high precision in one single infiltration run for each alloy composition.

The present data confirm findings of an earlier investigation in that drainage curves show two regions, namely one in which percolation governs infiltration, followed by another in which local pore characteristics dominate. The former obeys a universal scaling law, while in the second, the Brooks and Corey relation is obeyed.

It is also confirmed that in the initial percolation-dominated stage of infiltration, the metal traces a fractal of dimension D near 2.6, consistent with percolation theory (which predicts $D = 2.52$).

Adding tin to copper facilitates pressure infiltration of alumina by shifting the drainage curve homothetically to lower pressures. The reason for this is, in this system, that alloying reduces the melt surface tension, leaving the contact angle relatively constant. As a result, scaling of the drainage curves by the work of immersion or by the surface tension, indifferently, collapses all drainage curves onto one another, as one would expect from elementary physical reasoning.

Finally, it is found that the total work required for slow infiltration equals within 20 % the thermodynamic work for reversible infiltration of the present alumina particle preforms.

Acknowledgements This work was sponsored by the Swiss Foundation, Project No. 200020-137685. We gratefully acknowledge E. Berodier (EPFL) for the mercury intrusion porosimetry measurement, Willy Dufour, Raphael Charvet, Claudio Bacciarini, Cyril Dénéréaz and Dr. Noelia Calderon for their assistance in the design and construction of the infiltration apparatus used here, and Prof. W.C. Carter, of the Massachusetts Institute of Technology, for stimulating discussions.

References

1. Adamson AW (1982) Physical chemistry of surfaces, 4th edn. Wiley, New York
2. Eustathopoulos N, Nicholas MG, Drevet B (1999) Wettability at high temperature. Pergamon-Elsevier Science, Amsterdam
3. deGennes PG, Brochard-Wyart F, Quéré D (2004) Capillarity and wetting penomena: drops, bubbles, pearls, waves, Springer, New York (trans: Reisinger A)
4. Eustathopoulos N, Mortensen A (1993) In: Suresh S, Mortensen A, Needleman A (eds) Fundamentals of metal matrix composites. Butterworth-Heinemann, Stoneham, pp 42–58
5. Mortensen A, Jin I (1992) Solidification processing of metal matrix composites. Int Mater Rev 37:101–128
6. Michaud VJ (1993) In: Suresh S, Mortensen A, Needleman A (eds) Fundamentals of metal matrix composites. Butterworth-Heinemann, Stoneham, pp 3–41
7. Lloyd DJ, Morris AD, Jin I (1991) Melt process for the production of metal matrix composite materials with enhanced particle/matrix wetting. U.S 5,028,392
8. Mortensen A (2000) In: Clyne TW (ed) Comprehensive composite materials, vol 3. Pergamon, Oxford, pp 521–554
9. Asthana R (1998) Solidification processing of reinforced metals. Trans-Tech Publications, Uetikon-Zurich
10. Evans A, SanMarchi C, Mortensen A (2003) Metal matrix composites in industry: an introduction and a survey. Kluwer Academic Publishers, Dordrecht

11. Michaud V, Mortensen A (2001) Infiltration processing of fibre reinforced composites: governing phenomena. Compos A 32:981–996. doi:10.1016/S1359-835X(01)00015-X
12. Gutowski TG (1997) Advanced Composite Manufacturing. Wiley, New York
13. Sastry AM (2000) In: Anthony K, Carl Z (eds) Comprehensive composite materials, vol 2. Pergamon, Oxford, pp 609–622
14. Bourban PE (2000) In: Kelly A, Zweben C (eds) Comprehensive composite materials, vol 2. Pergamon, Oxford, pp 965–977
15. Clyne TW (2000) Comprehensive composite materials, vol 3. Pergamon, Oxford, pp 1–842
16. Bhatti AR, Farries PM (2000) In: Kelly A, Zweben C (eds) Comprehensive composite materials, vol 4. Pergamon, Oxford, pp 645–667
17. Parnas R (2000) Liquid composite molding. Hanser Gardner Publications, Cincinnati
18. Garcia-Cordovilla C, Louis E, Narciso J (1999) Pressure infiltration of packed ceramic particulates by liquid metals. Acta Mater 47(18):4461–4479. doi:10.1016/S1359-6454(99)00318-3
19. Chawla N, Chawla KK (2006) Metal matrix composites. Springer, New York
20. Taya M, Arsenault RJ (1989) Metal matrix composites: thermomechanical behavior. Pergamon Press, Oxford
21. Adam NK (1941) The physics and chemistry of surfaces, third edition. Republished in 1968 by Dover Publications, New York, USA
22. Morrow NR (1970) Physics and thermodynamics of capillary action in porous media. Ind Eng Chem 62:32–56. doi:10.1021/ie50726a006
23. Bear J (1972) Dynamics of fluids in porous media. American Elsevier, New York
24. Michaud VJ, Compton L, Mortensen A (1994) Capillarity in isothermal infiltration of alumina fiber preforms with aluminium. Metall Trans A 25:2145–2152. doi:10.1007/BF02652315
25. Bahraini M, Weber L, Narciso J, Mortensen A (2005) Wetting in infiltration of alumina particle preforms with molten copper. J Mater Sci 40:2487–2491. doi:10.1007/s10853-005-1980-1
26. Léger A, Calderon NR, Charvet R et al (2012) Capillarity in pressure infiltration: improvements in characterization of high-temperature systems. J Mater Sci 47:8419–8430. doi:10.1007/s10853-012-6645-2
27. Dullien FAL (1979) Porous media, fluid transport and pore structure. Academic Press, New York
28. Hunt A, Ewing R (2009) Percolation theory for flow in porous media. Springer, Heidelberg
29. Sahimi M (2011) Flow and transport in porous media and fractured rock: from classical methods to modern approaches, 2nd edn. Wiley-VCH Verlag, Germany
30. Mortensen A (1991) Interfacial phenomena in the solidification processing of metal matrix composites. Mater Sci Eng A 135:1–11. doi:10.1016/0921-5093(91)90527-T
31. Bahraini M (2007) Characterization of capillary forces during liquid metal infiltration, EPFL doctoral thesis 3787. Ecole Polytechnique Fédérale de Lausanne, Lausanne
32. Molina J, Bahraini M, Weber L, Mortensen A (2008) Direct measurement of drainage curves in infiltration of SiC particle preforms: influence of interfacial reactivity. J Mater Sci 43:5061–5068. doi:10.1007/s10853-008-2670-6
33. Léger A, Molina JM, Weber L, Mortensen A (2014) Percolation and universal scaling in composite infiltration processing, Mater Res Lett (in print)
34. Kaufmann H, Mortensen A (1992) Wetting of Saffil^{TM} alumina fiber preforms by aluminum at 973 K. Metall Trans A 23:2071–2073. doi:10.1007/BF02647554
35. Amore S, Ricci E, Lanata T, Novakovic R (2008) Surface tension and wetting behaviour of molten Cu–Sn alloys. J Alloy Compd 452:161–166. doi:10.1016/j.jallcom.2007.01.178
36. Lee J, Shimoda W, Tanaka T (2004) Surface tension and its temperature coefficient of liquid Sn-X (X = Ag, Cu) alloys. Mater Trans 45:2864–2870. doi:10.1088/0957-0233/16/2/015
37. Bahraini M, Molina JM, Kida M, Weber L, Narciso J, Mortensen A (2005) Measuring and tailoring capillary forces during liquid metal infiltration. Curr Opin Solid State Mater Sci 9:196–201. doi:10.1016/j.cossms.2006.02.007
38. Lenormand R (1989) Flow through porous media: limits of fractal patterns. Proc R Soc Lond A 423:159–168
39. Clément E, Baudet C, Hulin JP (1985) Multiple scale structure of non wetting fluid invasion fronts in 3D model porous media. J Phys Lett 46:1163–1171. doi:10.1051/jphyslet:0198500460240116300
40. Wilkinson D (1986) Percolation effects in immiscible displacement. Phys Rev A 34:1380–1391. doi:10.1103/PhysRevA.34.1380
41. Stauffer D, Aharony A (1994) Introduction to percolation theory—revised, 2nd edn. CRC Press, Boca Raton
42. Gouyet JF (1996) Physics and fractal structures. Masson, Paris and Springer, New York
43. Brooks RH, Corey AT (1964) Hydraulic properties of porous media, 3. Colorado State University Hydrology Papers
44. Dopler T, Modaressi A, Michaud VJ (2000) Simulation of metal composite isothermal infiltration processing. Metall Mater Trans B 31:225–233. doi:10.1007/s11663-000-0041-z
45. Rodriguez A, Sanchez S, Narciso J, Louis E, Rodriguez-Reinoso F (2005) Pressure infiltration of Al–Si alloys into compacts made of carbon particles. J Mater Sci 40:2519–2523. doi:10.1007/s10853-005-1985-9
46. Molina JM, Arpon R, Saravanan RA, Garcia-Cordovilla C, Louis E, Narciso J (2004) Threshold pressure for infiltration and particle specific surface area of particle compacts with bimodal particle distributions. Scr Mater 51:623–627. doi:10.1016/j.scriptamat.2004.05.009
47. Kida M, Bahraini M, Molina JM, Weber L, Mortensen A (2008) High-temperature wettability of aluminum nitride during liquid metal infiltration. Mater Sci Eng A 495:197–202. doi:10.1016/j.msea.2007.12.050
48. Krüger C, Mortensen A (2012) Al_2O_3 particle rounding in molten copper and Cu8 wt%Al. J Mater Sci 47:6346–6353. doi:10.1007/s10853-012-6559-z
49. Mortensen A, Cornie JA (1987) On the infiltration of metal matrix composites. Metall Trans A 18:1160–1163. doi:10.1007/BF02668570
50. Michaud V, Mortensen A (2007) On measuring wettability in infiltration processing. Scr Mater 56:859–862. doi:10.1016/j.scriptamat.2007.02.002
51. Michaud V, Mortensen A (2012) Corrigendum to: "On measuring wettability in infiltration processing" [Scripta Mater 56 (2007) 859-862]. Scr Mater 67:519–520. doi:10.1016/j.scriptamat.2012.06.001
52. Molina JM, Rodriguez-Guerrero A, Bahraini M et al (2007) Infiltration of graphite preforms with Al–Si eutectic alloy and mercury. Scr Mater 56:991–994. doi:10.1016/j.scriptamat.2007.01.042
53. Bahraini M, Molina JM, Weber L, Mortensen A (2008) Direct measurement of drainage curves in infiltration of SiC particle preforms. Mater Sci Eng A 495:203–207. doi:10.1016/j.msea.2008.01.074
54. Mortensen A, Wong T (1990) Infiltration of fibrous preforms by a pure metal: Part III. Capill phenom Metall Trans A 21A:2257–2263. doi:10.1007/BF02647888

55. Oya M, Takashi M, Iwata Y et al (2002) Mercury determines pore-size distribution intrusion porosimetry. Am Ceram Soc Bull 81:52–56
56. León y León CA (1998) New perspectives in mercury porosimetry. Adv Colloid Interfac 76–77:341–372. doi:10.1016/S0001-8686(98)00052-9
57. Keene BJ (1993) Review of data for the surface tension of pure metals. Inter Mater Rev 38:157–192. doi:10.1179/imr.1993.38.4.157